PHYSICAL REVIEW B VOLUME 47, NUMBER 19 15 MAY 1993-I

Tunneling measurements of symmetric-interface phonons in GaAs/AlAs double-barrier structures

P. J. Turley, C. R. Wallis, and S. W. Teitsworth
Department of Physics, Box 90305, Duke University, Durham, North Carolina 27708-0305

W. Li and P. K. Bhattacharya
Department of Electrical Engineering and Computer Science, University of Michigan, Ann Arbor, Michigan 48109
(Received 18 December 1992)

In this paper we report the results of extensive magnetotransport experiments on asymmetric GaAs/AlAs double-barrier structures that were specifically designed to possess large phonon-assisted tunneling currents. We find *quantitative* agreement between measured valley currents at liquid-helium temperature and calculations that include the effects of phonon localization using the dielectric-continuum model. The results demonstrate that (1) a major part of the valley current in these structures is due to phonon-assisted tunneling, and (2) symmetric-interface phonons and confined phonons in the GaAs well are the most important in phonon-assisted tunneling processes. Charge buildup in the GaAs well is found to shift current-voltage curves to higher voltages and to distort magnetic field versus applied voltage diagrams.

I. INTRODUCTION

Double-barrier resonant-tunneling structures are the focus of much current research, both for their potential application as high-speed devices as well as for their unique physical properties.[1] One critical issue for researchers is the magnitude of the excess current—also called the valley current—that flows through these structures for voltages just above resonance. A low valley current is desirable for most device applications, and quantitative modeling of this feature provides an ongoing challenge to theorists.

The valley current in GaAs/AlAs double-barrier structures has generally been attributed to several processes, including elastic scattering of tunneling electrons by impurities and interface roughness,[2–6] quasielastic scattering by acoustic phonons,[4] Γ-X conversion in AlAs barriers,[7,8] and inelastic scattering by longitudinal-optical (LO) phonons. In many structures, this last process causes phonon-assisted tunneling, in which electronic states in the emitter are coupled to the resonant state in the well through the emission of an optical phonon. This provides the electrons with an additional pathway for tunneling through the structures, leading to "satellite" peaks in current-voltage curves at low temperatures.[9]

Magnetotunneling data[10–14] suggest that the phonon-assisted tunneling current can be attributed to at least two types of phonons, one with the approximate energy of bulk GaAs LO phonons (36.2 meV), and the other with the energy of bulk AlAs LO phonons (50.1 meV).[10–13] However, much of the early theoretical research on phonon-assisted tunneling did not attempt to explain these results, in part due to uncertainty over how to model optical phonons in heterostructures.[4,14–20] In GaAs/AlAs heterostructures, it is now widely accepted that optical phonons can become localized, either in one of the semiconducting layers (confined phonons), or near the interface between two layers (interface phonons).[21–27] In previous papers,[16–18] we predicted that two types of phonon modes should dominate the current: confined phonons in the well, with an energy of 36.2 meV, and symmetric-interface phonons, with an energy of 50.1 meV in the long-wavelength limit. The properties of these modes were calculated using the dielectric-continuum model, a relatively simple macroscopic model of localized phonons which accurately approximates detailed microscopic models.[24] This is especially true for long-wavelength phonons, which are the ones most relevant in phonon-assisted tunneling.[18]

In this paper, we present tunneling and magnetotunneling data for an asymmetric GaAs/AlAs double-barrier structure which—when interpreted in terms of the dielectric-continuum model—demonstrate that a major part of the valley current in the structure is due to phonon-assisted tunneling via localized modes. In Sec. II, we review the theoretical calculations of phonon-assisted tunneling current, taking into account the two-dimensional nature of the emitter electronic states and charge buildup in the well. In Sec. III, we discuss sample structure, growth parameters, and processing steps, and show experimental current-voltage curves in the absence of an applied magnetic field. In Sec. IV, we discuss experimental current-voltage curves with an applied magnetic field parallel to current flow, from which we construct detailed diagrams showing the location of current peaks versus magnetic field and applied voltage.

II. CALCULATION OF PHONON-ASSISTED TUNNELING CURRENT

The composition of the double-barrier structure studied in this paper is shown in Table I. The core of the structure consists of an 80-Å undoped GaAs well surrounded by a 33-Å undoped AlAs barrier on the emitter side (under positive bias) and a 45-Å undoped AlAs barrier on the collector side. Spacer layers with a graded

TABLE I. Growth parameters for the experimental double-barrier structure.

Layer	Thickness	Composition
Cap	1.0 μm	GaAs (Si doped) $N_D=10^{18}$ cm^{-3}
	300 Å	GaAs (Si doped) $N_D=2\times10^{17}$ cm^{-3}
	300 Å	GaAs (Si doped) $N_D=4\times10^{16}$ cm^{-3}
	300 Å	GaAs (Si doped) $N_D=10^{16}$ cm^{-3}
	50 Å	GaAs (undoped)
Collector barrier	45 Å	AlAs (undoped)
Well	80 Å	GaAs (undoped)
Emitter barrier	33 Å	AlAs (undoped)
	50 Å	GaAs (undoped)
	300 Å	GaAs (Si doped) $N_D=10^{16}$ cm^{-3}
	300 Å	GaAs (Si doped) $N_D=4\times10^{16}$ cm^{-3}
	300 Å	GaAs (Si doped) $N_D=2\times10^{17}$ cm^{-3}
	2 μm	GaAs (Si doped) $N_D=2\times10^{18}$ cm^{-3}
Substrate		n^+ GaAs substrate ⟨100⟩ direction

doping profile on either side of the structure ensure the formation of a two-dimensional launching state for electrons. The calculated current densities discussed in this section are scaled to 250-μm-diameter mesas, which were the focus of the experimental measurements (see Sec. III).

Figure 1(a) shows the calculated conduction-band-edge profile of the double-barrier structure for an applied voltage just above the resonant-tunneling voltage. The profile in the emitter (left) side is calculated by solving the Poisson and Schrödinger equations self-consistently with $T=0$. Since the experimental current densities are reasonably small, we assume the effect of current flow on the potential profile in the emitter is small. The voltage drop across the collector space layer is calculated using a standard depletion-layer approximation, once again neglecting the effect of current flow on the profile.[28] In Fig. 1, we have neglected charge buildup in the well, though this will be considered below.

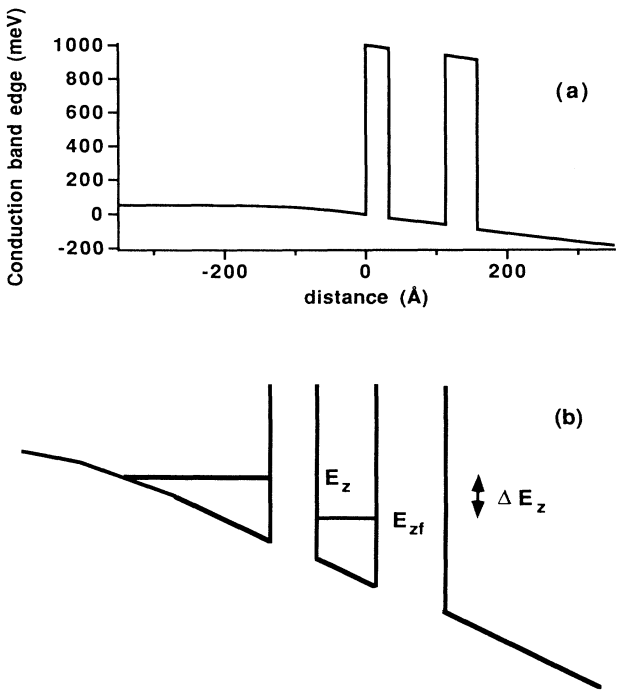

FIG. 1. (a) The calculated conduction-band-edge profile for the device structure under applied bias. (b) Detail showing the emitter state in the accumulation layer, the resonant state in the well, and the energy loss ΔE_z.

At low temperatures, most of the electrons in the emitter are found in the lowest two-dimensional energy state with a z energy E_z, as shown in Fig. 1(b). (Excited states in the emitter can be important at room temperature and 77 K, but will not contribute to current in these experiments.[29,30]) In order for current to flow, electrons must be transferred from the emitter state at E_z to the resonant state in the well denoted by E_{zf}. When $E_z \approx E_{zf}$, the overlap between the two states couples them strongly giving rise to the resonant-tunneling current. When $E_z > E_{zf}$, electrons in the emitter can be coupled to the resonant state in the well through the emission of an optical phonon. Once in the resonant state, the electron has a negligible probability of reabsorbing the phonon (at low temperatures), and eventually tunnels out through the collector barrier, leading to a second peak in the current for voltages above the resonant-tunneling value.

The phonon-emission rate can be calculated using the Fermi golden rule:

$$W(i\rightarrow f)=\frac{2\pi}{\hbar}|\langle f|H_{e\text{-ph}}|i\rangle|^2\delta(E_i-E_f-\hbar\omega_0)\ , \qquad (2.1)$$

where $H_{e\text{-ph}}$ is the electron-phonon Hamiltonian, E_i is the energy of the initial electronic state, E_f is the energy of the final electronic state, and $\hbar\omega_0$ is the energy of the emitted phonon. The *total* initial state $|i\rangle$ has one electron in the state Ψ_i with no phonons, while the *total* final state consists of one electron in the state Ψ_f plus one emitted phonon.

The electronic states are calculated using a transfer-matrix routine.[31] We use an AlAs barrier height of 1.0 eV, and the tunneling effective mass of the electrons in AlAs is taken to be $0.09m_0$, where m_0 is the free-electron mass. This is significantly below the conduction-band-edge value of $0.15m_0$, but it is more consistent with recent theory and experimental data based on cyclotron

resonance measurements[32] and resonant-tunneling measurements.[33]

The electron-phonon Hamiltonians are calculated using the dielectric-continuum model, wherein the properties of localized phonon modes are derived using the bulk dielectric properties of the semiconductor layers. In previous papers, we have predicted that two types of localized phonons are most important for determining phonon-assisted tunneling currents in typical double-barrier structures: confined phonons in the well, which have the energy of bulk GaAs LO phonons (36.2 meV), and symmetric-interface phonons, which in the long-wavelength limit have the energy of bulk AlAs LO phonons (50.1 meV). These are called the "inner" symmetric modes in Ref. 18 (because the associated electrostatic potentials peak at the inner pair of heterointerfaces), and are labeled ω_{s2+} in Ref. 25. The electron-phonon Hamiltonian for the confined mode has been given in Ref. 18, while the Hamiltonian for the interface mode has been given in Ref. 25.

In this paper, we do *not* make the long-wavelength approximation that was discussed in some of the previous work.[16–18] For the "inner" symmetric-interface modes, the long-wavelength approximation overestimates the current by about a factor of 2.

The emission rate is summed over all available initial and final states in order to calculate the current. Previous treatments of phonon-assisted tunneling have typically assumed a three-dimensional density of states in the emitter,[4,16–18] but for this structure the current formula must reflect the two-dimensional nature of the electronic states in the emitter. The current is then given by

$$J(V)=\frac{e}{A}\int d\mathbf{k}'_{\parallel}\int d\mathbf{k}_{\parallel}W(i\rightarrow f;V) \times g_w(\mathbf{k}'_{\parallel})g_e(\mathbf{k}_{\parallel})f_e(\mathbf{k}_{\parallel})[1-f_w(\mathbf{k}'_{\parallel})] , \tag{2.2}$$

where $\mathbf{k}_{\parallel}$ is the initial momentum of the electron projected onto the plane of the interfaces, $\mathbf{k}'_{\parallel}$ is the final momentum of the electron projected onto the plane of the interfaces, $g_e(\mathbf{k}_{\parallel})=2(A/(2\pi)^2)$ is the density of electronic states in the emitter, $g_w(\mathbf{k}'_{\parallel})=(A/(2\pi)^2)$ is the density of available electronic states in the well (the factor of 2 is dropped because the electrons do not change spin during phonon emission), A is the cross-sectional area of the device, $f_e(\mathbf{k}_{\parallel})$ is the Fermi distribution of electrons in the emitter, and $f_w(\mathbf{k}'_{\parallel})$ is the Fermi distribution of electrons in the quantum well.

Figure 2(a) shows the result of a numerical evaluation of Eq. (2.2) for the phonon-assisted tunneling current of the device structure in forward bias (the 33-Å barrier as the emitter barrier) at zero temperature, with $f_w(\mathbf{k}'_{\parallel})$ set to zero. Curve (1) shows the current due to the emission of confined modes in the well with energy 36.2 meV. Curve (2) shows the current due to the emission of the symmetric-interface modes, while curve (3) shows the combined current. It is important to realize that the z-energy difference of the emitter and resonant states, $\Delta E_z=E_z-E_{zf}$, is not strictly equal to the phonon energy $\hbar\omega_0$. During the scattering process, the electron can change its parallel momentum from $\mathbf{k}_{\parallel}$ to $\mathbf{k}'_{\parallel}$, with the extra momentum taken up by the phonon: $\mathbf{k}_{\parallel}=\mathbf{k}'_{\parallel}+\mathbf{q}_{\parallel}$. The resulting formula for ΔE_z is

$$\Delta E_z=\hbar\omega_0+\frac{\hbar^2(k'^2_{\parallel}-k^2_{\parallel})}{2m^*} . \tag{2.3}$$

Thus, even though we included no broadening of the initial electronic levels for the calculation of Fig. 2(a), the phonon-assisted tunneling current is spread over a large range of voltages due to the three-dimensional nature of the emission process.

It is also important to note that the current due to confined modes (curve 1) decays slowly away from its peak value at 0.48 V with increasing voltage. Because the electron-phonon Hamiltonian for the confined mode[16,18] is proportional to $[q_{\parallel}^2+(\pi/d_1)^2]^{-1/2}$, and typically $q_{\parallel}<\pi/d_1$ (d_1 denotes the GaAs well width), the probability of emitting phonons with a large momentum in the parallel direction is not significantly smaller than that for emitting phonons with small momentum.

The calculations for Fig. 2(a) assume that electrons tunnel through the collector barrier so fast that there is no charge buildup in the well. However, if the collector barrier is thick enough, the charge may accumulate in the well, increasing the well occupation factor $f_w(\mathbf{k}'_{\parallel})$ and reducing the number of available final states.[34–38] Charge buildup also implies the presence of a space

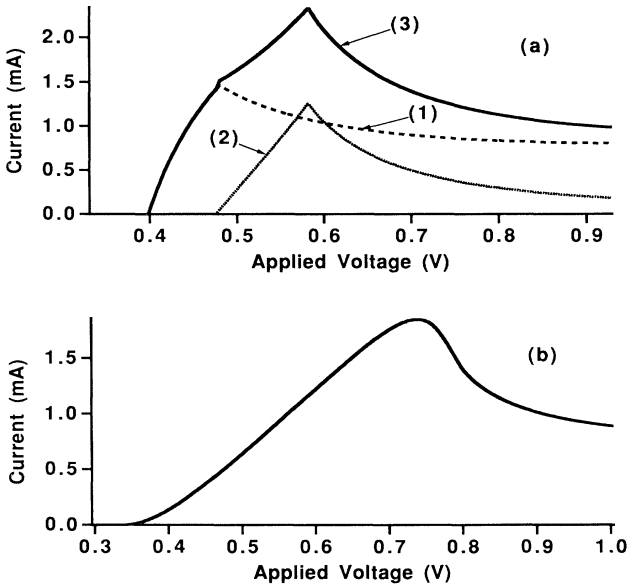

FIG. 2. (a) The calculated phonon-assisted tunneling current in the *forward* bias direction, with no broadening and no charge buildup in the well. Curve 1: The current due to emission of confined modes in the well $\hbar\omega_0=36.2$ meV. Curve 2: The current due to emission of symmetric-interface modes $\hbar\omega_0\approx 50.1$ meV. Curve 3: The total phonon-assisted tunneling current. (b) The calculated phonon-assisted tunneling current in the forward bias direction, including the effects of charge buildup and 5-meV broadening of the emitter electronic state.

charge which may significantly distort the conduction-band-edge profile, leading to a shift of peak voltages to higher values.

Once an electron emits a phonon and drops into the resonant state, it will remain in the well before tunneling through the collector barrier in a characteristic time τ_w. For our structure, with a 45-Å collector barrier, this time is estimated to be about 5 ns.[39] (It may be much smaller in structures with thin barriers.) Because the acoustic-phonon-emission rate is many times faster, typically <0.1 ns,[40] it is reasonable to assume that the electrons in the well quickly relax to the lattice temperature once they have dropped into the resonant state. The well occupation factor $f_w(\mathbf{k}'_\parallel)$ is then given by ($T=0$)

$$f_w(\mathbf{k}'_\parallel)=\begin{cases}1 & k'_\parallel<k_F\\ 0 & k'_\parallel>k_F\end{cases},$$

where (2.4)

$$k_F=\left[\frac{2\pi\tau_w J}{e}\right]^{1/2}$$

Here k_F is the effective two-dimensional Fermi wave vector in the well. Since the current density J is dependent on the amount of charge in the well, $f_w(\mathbf{k}'_\parallel)$ must be calculated self-consistently.

Although we have seen that the phonon-assisted tunneling current spreads over a range of voltages without including electronic-state broadening, broadening of the two-dimensional emitter state plays an important role in real structures, smoothing sharp features in the curves of Fig. 2(a). Electron-electron and electron–LO-phonon scattering have relaxation times on the order of 100 fs,[41,42] which in light of the energy-time uncertainty relation implies that the electronic states possess inelastic broadening Γ_i of about 5 meV. We have found that the current-voltage curves are insensitive to the exact value of Γ_i, so that any value between 3 and 8 meV gives similar results.

In Fig. 2(b), we have self-consistently calculated the phonon-assisted tunneling curve for the forward bias, taking into account the effects of charge buildup in the well and with $\Gamma_i=5$ meV. The current levels are slightly lower than in Fig. 2(a), since the charge buildup in the well reduces the number of available final states. The peak position has also been shifted from ≈ 0.58 to ≈ 0.75 V, due to the band bending induced by the space charge in the GaAs well.

In Fig. 3(a), we have calculated the phonon-assisted tunneling current of the structure under reverse bias (the 45-Å barrier as the emitter barrier) with $f_w(\mathbf{k}'_\parallel)$ and Γ_i set to zero. The current levels are much smaller in the reverse bias direction because, when the effects of charge buildup are ignored, the phonon-assisted tunneling current is essentially dependent only on the width of the emitter barrier, through which the initial and final states couple. In the reverse bias direction, the effects of charge buildup are relatively minor, since the electrons tunnel out quickly through the thin (33-Å) collector barrier. In Fig. 3(b), we have calculated the phonon-assisted tunneling current including the effects of charge buildup, and

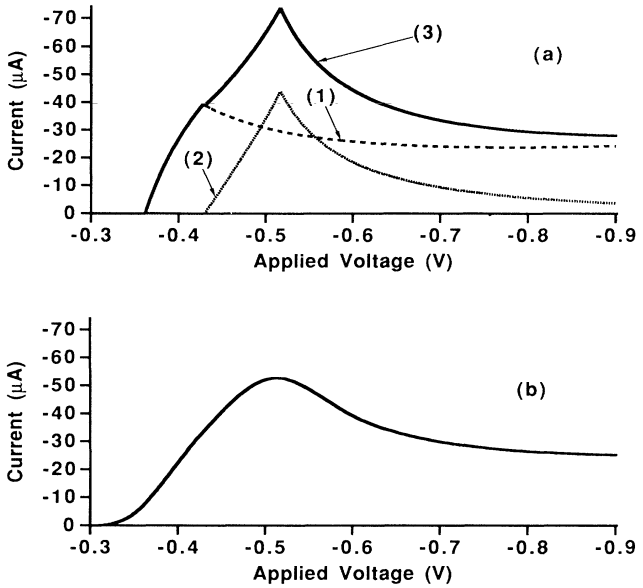

FIG. 3. (a) The calculated phonon-assisted tunneling current in the *reverse* bias direction, with no broadening and no charge buildup in the well. Curve 1: The current due to emission of confined modes in the well. Curve 2: The current due to emission of symmetric-interface modes. Curve 3: The total phonon-assisted tunneling current. (b) The calculated phonon-assisted tunneling current in the reverse bias direction, including the effects of charge buildup and 5-meV broadening of the emitter electronic state.

with $\Gamma_i=5$ meV. Note that in this case the resonant peak is not shifted to a higher voltage and, while the peak current is slightly lower, the areas under the curves in Figs. 3(a) and 3(b) are similar.

III. TUNNELING EXPERIMENTS

The experimental structure was grown by molecular-beam epitaxy (MBE) using a Varian GEN II on an n^+-GaAs(100)-oriented substrate, as shown in Table I with a substrate temperature of approximately 580 °C. Growth interrupts of 90 s were used when switching from AlAs growth to GaAs growth, but no interrupts were used when switching from GaAs to AlAs. The unintentional background doping is p type, with a concentration estimated to be $\sim 10^{14}$ cm^{-3}. Ohmic contacts consisting of 400 Å of Ge followed by 300 Å of Ni and 1400 Å of Au were evaporated onto the sample through a shadow mask. The contacts were annealed in a rapid thermal annealer at 360 °C for 1 min in a pure N_2 atmosphere. Contacts were then used as a mask for wet mesa etching in a 7:2:1 mixture of $[H_2O]$:$[H_2O_2]$:$[H_3PO_4]$.

Several different mesas were examined at temperatures from 1.5 to 300 K. Results shown here are for 250-μm-diameter mesas at 4.2 K. As expected, larger 500-μm-diameter mesas possessed current levels scaled up by ~ 4 relative to 250-μm results, and also exhibited unstable current oscillations above the phonon-assisted tunneling peak due to larger capacitance of the device.

Two gold wires, one for the current leads and one to

measure the voltage across the sample, were attached to each mesa using an ultrasonic wire bonder. The back side of the sample was fixed onto a small copper plate using silver paint, and two leads were attached to the plate. The voltage across the sample was supplied by a Keithley 230 programmable voltage source and was monitored by Keithley 175 digital multimeters, one connected to each voltage lead. The current was measured by monitoring the voltage across a 10.00-Ω resistance in series, with the current leads using a Keithley 197 microvolt digital multimeter. Detailed I-V curves for these structures were also measured at 1.5 K, but differed insignificantly from the 4.2-K results.

Figure 4(a) shows a typical I-V curve for these samples at 4.2 K. In forward bias (the 33-Å barrier as the emitter barrier), the main resonant-tunneling peak is at ≈ 0.54 V. This is followed by the phonon-assisted tunneling peak at ≈ 0.81 V. The presence of this unusually large phonon-assisted tunneling peak is due in part to the unequal barrier-layer thicknesses. In fact, strong phonon-assisted tunneling peaks have also been reported in asymmetric $GaAs/Al_{0.4}Ga_{0.6}As$ double-barrier structures.[36,38] The small plateau observed in the I-V curves for voltages just above the resonant-tunneling peak corresponds to time averages of the oscillating current.

In the reverse bias direction, the main resonant-tunneling peak is seen at ≈ -0.24 V, followed by another plateau associated with external circuit oscillations. The phonon-assisted tunneling peak at ≈ -0.48 V is much smaller than in the forward bias case. In each bias direction, the hysteresis observed near the plateau regions is too small to be depicted on this graph.

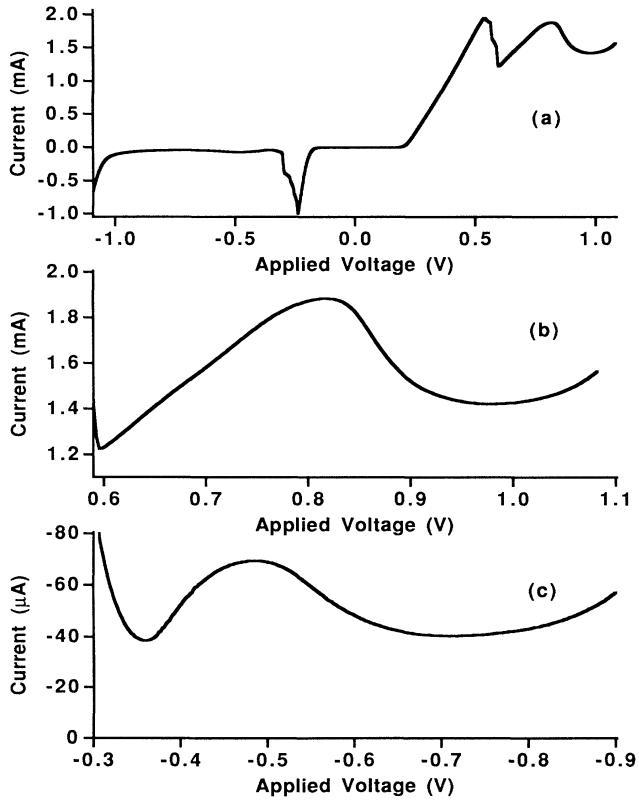

FIG. 4. (a) The experimentally measured current-voltage curve with no applied magnetic field. (b) The expansion of Fig. 4(a) focusing on the phonon-assisted tunneling peak in the *forward* bias direction. (c) An expansion of Fig. 4(a) focusing on the phonon-assisted tunneling peak in the *reverse* bias direction.

Figure 4(b) shows an enlargement of the experimental current voltage curve near the forward bias phonon-assisted tunneling peak. This is in good quantitative agreement with the calculated curve of Fig. 2(b). The peak voltages differ by 8.7% [0.745 (theory) versus 0.816 V (experiment)], while the peak currents differ by only 2.5% [1.93 (theory) versus 1.88 mA (experiment)], a remarkable fit for a calculation with essentially no adjustable parameters.

Above 1.0 V, the experimental current increases rapidly. Since tunneling through the second resonant state in the well is not expected to occur until ≈ 1.5 V, this rapid increase is most likely due to tunneling over the X point in the AlAs collector barrier,[7] and probably accounts for most of the discrepancy between theory and experiment for voltages above 0.85 V.

Figure 4(c) shows an enlargement of the experimental current-voltage curve near the phonon-assisted tunneling peak in the reverse bias direction. In this case the agreement in voltage is closer, 5.7% [−0.513 (theory) versus −0.485 V (experiment)], while the agreement in current is not as accurate, 24% [−52.8 (theory) versus −69.5 μA (experiment)]. Note that the excess current at −0.7 V in theory and experiment is quite similar, indicating that even for voltages well beyond the phonon peak, most of the excess current in this device can be explained as phonon-assisted tunneling. Once again, below −0.9-V tunneling over the X point in the collector barrier leads to a rapid increase in current.

IV. MAGNETOTUNNELING DATA

We expect that the phonon peaks for both forward and reverse biases are due to two types of phonons, i.e., the confined modes in the well with an energy of 36.2 meV and the symmetric interface modes with an energy of 50.1 meV. With no applied magnetic field, the contributions from the two phonon types are difficult to resolve without differentiating I-V curves, as seen in the preceding theoretical and experimental results. This is due to the fact that the energy loss in the z direction, ΔE_z, is not equal to the energy of the phonons, $\hbar\omega_0$, but is also affected by the energy changes in the directions parallel to the interfaces as in Eq. (2.3). On the other hand, when a magnetic field is applied in the z direction—parallel to current flow—the electronic energies in the x-y directions are quantized into Landau levels with energy $\hbar\omega_c(\nu+\frac{1}{2})$, where ω_c is the cyclotron frequency $\omega_c = eB/m^*$, and $\nu = 0, 1, 2, \ldots$ is the Landau level number. The energy loss in the z direction is then given by

$$\Delta E_z = \hbar\omega_0 + \hbar\omega_c(\Delta\nu) , \tag{4.1}$$

where $\Delta\nu$ is the change in the Landau level caused by the optical-phonon emission. Thus ΔE_z is quantized into discrete steps, making it more straightforward to separate

out contributions from confined and interface modes.

Figures 5(a)–5(c) show experimental current-voltage curves for the phonon-assisted tunneling peak in the forward bias direction for three different magnetic fields. These traces are all taken with increasing voltage. I-V curves taken with decreasing voltage are only slightly different due to a small amount of hysteresis. Although this hysteresis is slightly enhanced with increasing magnetic field, it is not as pronounced as that reported by Leadbeater and Eaves for $GaAs/Al_{0.4}Ga_{0.6}As$ structures.[38] At 2.81 T, the phonon-assisted tunneling curve is slightly scalloped. Each one of these peaks corresponds to a different type of Landau-level transition. As the magnetic field is increased, $\hbar\omega_c$ becomes larger and the peaks proportionally spread out in voltage. At 7.18 T, the peaks are sharp and quite prominent. On the other hand, the main resonant-tunneling peak (not shown) possesses only slight shape variations with applied magnetic field, since—with the exception of relatively weak elastic-scattering events—the momentum parallel to the interfaces is conserved during resonant tunneling.

Each peak in the magnetic-field traces should be attributable to a particular type of Landau-level transition. This can by done by plotting a diagram in which the location of each peak is plotted versus magnetic field and voltage. The location of the current peaks is best determined from the minima of the second derivative d^2I/dV^2. At larger magnetic fields (>2 T), we determined d^2I/dV^2 by computing the second derivative of the current-voltage curves, while at lower magnetic fields the differential conductivity of the sample was measured directly using a lock-in technique which provided enhanced sensitivity. This technique consisted in applying a dc voltage plus a small ac signal to the sample circuit with the ac component of the voltage δV across the sample measured by a lock-in amplifier (Stanford model SR-510). A second lock in (Stanford model SR-530) measured the ac current signal δI by monitoring the ac voltage across a precision resistance in series with the current leads. A first derivative of the resultant conductivity data was then computed to obtain d^2I/dV^2 vs dc voltage V.

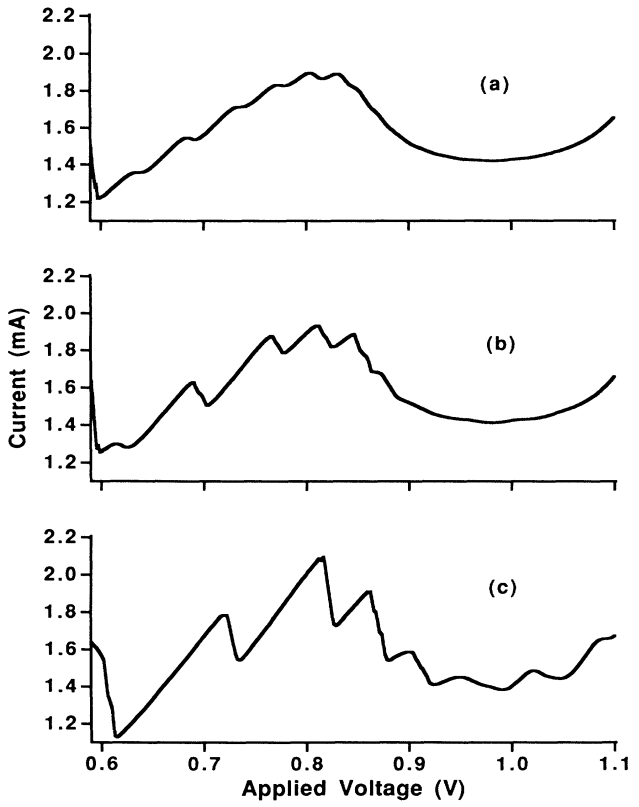

FIG. 5. Experimentally measured current-voltage curves with different magnetic fields, focusing on the phonon peak under *forward* bias: (a) 2.81, (b) 4.56, and (c) 7.18 T.

The derivatives were taken using a numerical digital filter.[43] The initial data points b_k were convoluted with a differentiating filter using Lanczos smoothing according to the following prescription:

$$d_i = \sum_{k=-N}^{N} b_{i+k} c_k \ , \tag{4.2}$$

$$c_k = \mathrm{sgn}(k) \frac{\sin(\pi k/N)}{(\pi k/N)} \frac{2}{\pi} \times \left[\frac{\sin(k\omega_{co})}{k^2} - \frac{\omega_{co}\cos(k\omega_{co})}{k} \right] .$$

Here d_i denotes the desired derivative, ω_{co} is the cutoff frequency, N is the number of points in the digital filter, and $\mathrm{sgn}(k)$ returns the sign of k. The parameters N and ω_{co} were optimized in order to reduce noise while retaining small features. For our data, the number of points in the filter was typically set at $N=10$, while the optimum value of ω_{co} was found to be 0.3.

In Figs. 6(a) and 6(b), we show magnetic field versus applied voltage diagrams for the forward bias phonon peak. There are two distinct "Landau fan" patterns which converge as the magnetic field is reduced to zero. One pattern converges to 0.67 V and corresponds to the emission of confined modes in the well while the other pattern converges to 0.81 V and corresponds to the emission of symmetric-interface modes. At low magnetic field, the patterns are quite regular, without any of the systematic deviations from straight patterns that were predicted in Ref. 17 on the assumption of a three-dimensional emitter state. This provides strong evidence for the two-dimensional nature of the emitter state in these experimental structures. In different structures with reduced emitter-spacer-layer length, one might expect a more three-dimensional electron gas to form in the emitter, which would alter the low-field structure considerably. Magnetotunneling data thus appear to provide a useful method for determining effective dimensionality of the emitter electronic states.

Other researchers have observed patterns emanating from the resonant-tunneling peaks due to elastic-scattering events.[11,12] In our structure, those patterns are buried beneath the strong phonon-assisted tunneling peak, although the small section of the line above 4 T and below 0.65 V in Fig. 6(a) seems to be emanating from the resonant-tunneling peak. The absence of any strong structure associated with the resonant-tunneling peak provides further indication that most of the excess

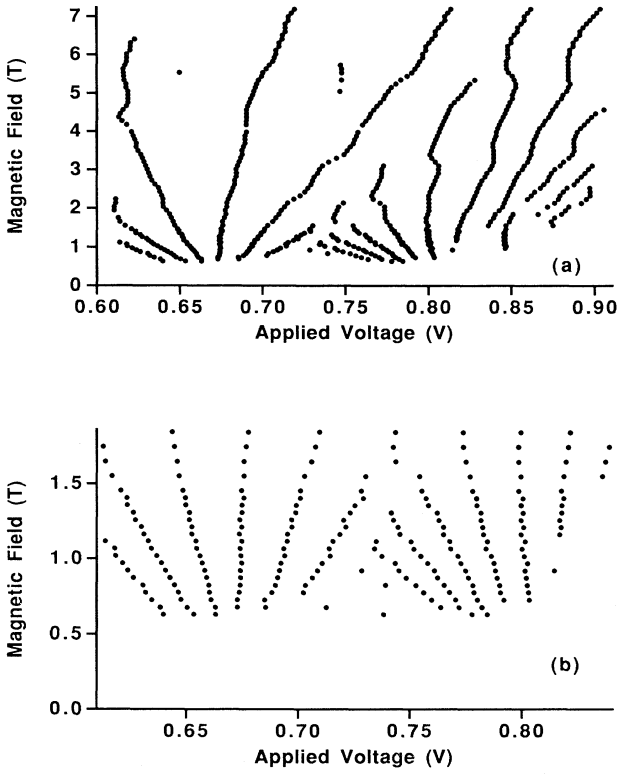

FIG. 6. Forward bias diagrams: voltage locations of current peaks vs magnetic field. (a) The full-field range, and (b) the low-field range.

current in this structure is due to phonon-assisted tunneling.

In Fig. 7, we show the magnetic field versus voltage diagram obtained with the sample under reverse bias. Since the current levels are much smaller in this direction, the patterns cannot be extended to as low a magnetic field as in the forward bias case. Nonetheless, we clearly observe two straight vertical lines that converge to -0.45 V and -0.52. These two lines correspond to the emission of confined and symmetric-interface modes, respectively, with no change in the Landau level. The other lines correspond to the emission of phonons with a change in the Landau-level index.

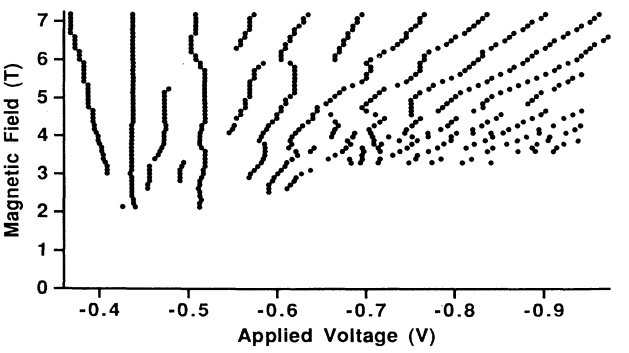

FIG. 7. The reverse bias diagram: voltage locations of current peaks vs magnetic field.

The differences between the forward and reverse bias diagrams reveal some of the consequences of charge buildup in the GaAs well. As the magnetic field is increased, the current peaks become higher and sharper[17] (see Fig. 5). In the forward bias case this significantly increases charge buildup in the well, and thus skews the patterns toward higher voltages as the magnetic field increases. Under reverse bias there is minimal charge buildup, so that the $\Delta\nu=0$ patterns are straight even at high magnetic fields. Finally, we note that in both Figs. 6 and 7 deviations from the straight lines are observed at level crossings, but these are unrelated to the *anticrossings* observed by Boebinger *et al.*, which occurred for much higher magnetic fields and were attributed by the authors to magnetopolaron effects.[11]

V. DISCUSSION

In conclusion, we have shown close agreement between the experimentally measured phonon-assisted tunneling current in GaAs/AlAs double-barrier structures and predictions based on a dielectric continuum model of localized phonons, demonstrating that most of the valley current can be attributed to optical-phonon-assisted tunneling at low temperatures. Symmetric interface phonons (with the energy of bulk AlAs LO phonons) and the confined-well phonons (with the energy of bulk GaAs LO phonons) are the most important, and contribute roughly equivalent amounts to the total current. Furthermore, we find that charge buildup in the well has two principal effects: (1) it reduces the number of available states in the well (via Pauli exclusion), which causes the phonon-assisted tunneling peak current to saturate (Fig. 5); and (2) it distorts the potential profile, which produces a skewing of current-voltage curves to higher voltages when the current is high. The latter effect is strikingly illustrated in the forward bias magnetic field versus voltage diagram [Fig. 6(a)].

Magnetotunneling measurements such as these hold promise as a viable method for performing spectroscopy of localized phonons and precisely determining the frequency of the different modes.[14] This requires calibration of the experimental voltage scale—which includes the potential drop across the large spacer layers—in terms of the electronic energy scale ΔE_z. Ideally, these are related by a current-independent constant parameter α so that $V=\alpha\Delta E_z$. However, for the present structure the large amount of charge buildup in the well under forward bias means that V and ΔE_z are no longer related by a simple constant (i.e., a α becomes dependent on current), so that an accurate spectroscopy is somewhat complicated. On the other hand, under reverse bias there is relatively little charge buildup in the well, and the scaling between voltage and energy scales is expected to be linear. The parameter α can then easily be determined from the slopes of the reverse bias magnetic-field diagrams (Fig. 7) using Eq. (4.1). On the basis of the first six lines, we estimate $\alpha=5.49\pm0.15$ V/eV, which, referring to the voltage difference between the resonant-tunneling peak and the two phonon-assisted tunneling peaks, gives

$\hbar\omega_0 = 36.0 \pm 0.9$ meV for the confined phonons, and $\hbar\omega_0 = 50.3 \pm 1.3$ meV for the symmetric-interface phonons, well within the accepted bulk values of 36.2 and 50.1 meV.

The properties of double-barrier symmetric-interface modes were derived in Refs. 18 and 25, assuming that the emitter and collector AlAs barriers were of equivalent length. Although this is not the case for the structure measured here, we have calculated the full dielectric-continuum model Hamiltonian for our asymmetric structure and find that it differs only slightly from the approximate models used in the calculations of Sec. II. We have also neglected various effects of dynamic electron screening which might be expected to play a role in these structures *a priori*. Large electron concentrations in both the emitter layer and the GaAs well should alter the dielectric properties of those layers, affecting both the phonon-dispersion relations and the strength of electron-phonon coupling. While we have argued in a previous paper that the mobile charge in the emitter reduces the strength of the "outer" symmetric phonon modes (i.e., those modes with associated electrostatic potentials that peak at the outer pair of heterointerfaces),[18] the full effect of electron screening on phonon-assisted tunneling awaits further theoretical investigation.

In the full dielectric-continuum model for a double-barrier structure, there are a total of ten different types of localized optical-phonon modes. Calculations of the phonon-assisted tunneling rates for each of the ten modes have been carried out and suggest that all but four of these can be dismissed as relatively insignificant for phonon-assisted tunneling in typical double-barrier structures. Thus the confined phonons in the AlAs barriers do not overlap much with electronic wave functions—particularly the resonant state—and the resultant emission rate is quite small.[16,31] The four antisymmetric-interface modes have very small overlap with the electronic states (which are approximately symmetric with respect to the well center) and, additionally, possess vanishingly small electron-phonon-coupling constants in the long-wavelength limit.[16,22,25] The TO-like "inner" symmetric-interface phonons with an energy ≈ 33.3 meV—associated with the inner pair of heterointerfaces and labeled ω_{s1-} in Ref. 25—have a very small electron-phonon-coupling constant.

Four modes remain, two of which, the confined phonons in the well and the "inner" symmetric-interface phonons, have been the focus of this paper. The other two are the LO-like "outer" symmetric-interface phonons (energy ≈ 36.2 meV, labeled ω_{s1+} in Ref. 25) and the TO-like "outer" symmetric phonons with an energy ≈ 44.8 meV (labeled ω_{s2+} in Ref. 25). A preliminary calculation of the contribution of these two modes to the phonon-assisted tunneling current using the methods of Sec. II gives a contribution which approaches that of the confined well and "inner" symmetric-interface modes. While these modes may be important in some structures, we have not included them here for the following reasons: (1) both TO- and LO-like "outer" modes are expected to be strongly damped by the screening action of electrons in the emitter, thereby reducing their contribution to phonon-assisted tunneling; and (2) no experimental evidence for a TO-like phonon with energy 44.8 meV was observed in either I-V curves or magnetic field versus voltage diagrams.

ACKNOWLEDGMENTS

We thank R. Haque, K. W. Kim, R. Lake, and M. A. Stroscio for helpful conversations, and also acknowledge the support of the National Science Foundation through Grant Nos. DMR-9208381 and DMR-9157549.

[1] F. Beltram, F. Capasso, and S. Sen, in *Electronic Materials*, edited by J. R. Chelikowski and A. Franciosi (Springer-Verlag, Berlin, 1991).
[2] E. Wolak, K. L. Lear, P. M. Pitner, E. S. Hellman, B. G. Park, T. Weil, J. S. Harris, and D. Thomas, Appl. Phys. Lett. **53**, 201 (1988).
[3] H. C. Liu and D. D. Coon, J. Appl. Phys. **64**, 6785 (1988).
[4] F. Chevoir and B. Vinter, Appl. Phys. Lett. **55**, 1859 (1989).
[5] J. Leo and A. H. MacDonald, Phys. Rev. Lett. **64**, 817 (1990).
[6] J. D. Bruno and J. S. Hurley, Superlatt. Microstruct. **11**, 23 (1992).
[7] E. E. Mendez, E. Calleja, and W. I. Wang, Phys. Rev. B **34**, 6026 (1986).
[8] C. R. Bolognesi, R. S. Mand, and A. R. Boothroyd, Appl. Phys. Lett. **57**, 575 (1990).
[9] V. J. Goldman, D. C. Tsui, and J. E. Cunningham, Phys. Rev. B **36**, 7635 (1987).
[10] M. L. Leadbeater, E. S. Alves, L. Eaves, M. Henini, O. H. Hughes, A. Celeste, J. C. Portal, G. Hill, and M. A. Pate, Phys. Rev. B **39**, 3438 (1989).
[11] G. S. Boebinger, A. F. J. Levi, S. Schmitt-Rink, A. Passner, L. N. Pfeiffer, and K. W. West, Phys. Rev. Lett. **65**, 235 (1990).
[12] J. G. Chen, C. H. Yang, M. J. Yang, and R. Wilson, Phys. Rev. B **43**, 4531 (1991).
[13] R. E. Pritchard, P. C. Harness, L. Cury, J. C. Portal, B. Khamsehpour, W. S. Truscott, and K. W. Singer, Semicond. Sci. Technol. **6**, 629 (1991).
[14] Y. Galvao Gobato, F. Chevior, J. M. Berrior, P. Bois, Y. Guldner, J. Nagle, J. P. Vieren, and B. Vinter, Phys. Rev. B **43**, 4843 (1991).
[15] N. S. Wingreen, K. W. Jacobsen, and J. W. Wilkins, Phys. Rev. Lett. **61**, 1396 (1988).
[16] P. J. Turley and S. W. Teitsworth, Phys. Rev. B **44**, 8181 (1991).
[17] P. J. Turley and S. W. Teitsworth, Phys. Rev. B **44**, 12 959 (1991).
[18] P. J. Turley and S. W. Teitsworth, J. Appl. Phys. **72**, 2356 (1992).
[19] R. Lake and S. Datta, Phys. Rev. B **45**, 6670 (1992).
[20] A. Nogaret and J. C. Portal, Surf. Sci. **263**, 234 (1992).
[21] M. V. Klein, IEEE J. Quantum Electron. **QE-22**, 1760 (1986).
[22] N. Mori and T. Ando, Phys. Rev. B **40**, 6175 (1989).
[23] J. Menéndez, J. Lumin. **44**, 285 (1989).
[24] P. Lugli, E. Molinari, and H. Rüker, Superlatt. Microstruct. **10**, 471 (1991).
[25] K. W. Kim, A. R. Bhatt, M. A. Stroscio, P. J. Turley, and S.

W. Teitsworth, J. Appl. Phys. **72**, 2282 (1992).
[26]B. K. Ridley and M. Babiker, Phys. Rev. B **43**, 9096 (1991).
[27]K. J. Nash, Phys. Rev. B **46**, 7723 (1992).
[28]S. M. Sze, *Physics of Semiconductor Devices,* 2nd ed. (Wiley, New York, 1981).
[29]E. T. Koenig, B. Jogai, M. J. Paulus, C. I. Huang, and C. A. Bozada, J. Appl. Phys. **68**, 3425 (1990).
[30]J. Chen, J. G. Chen, C. H. Yang, and R. A. Wilson, J. Appl. Phys. **70**, 3131 (1990).
[31]P. J. Turley and S. W. Teitsworth, Phys. Rev. B **44**, 3199 (1991).
[32]G. Brozak, E. A. Andrada e Silva, L. J. Sham, F. DeRosa, P. Miceli, S. A. Schwarz, J. P. Harbison, L. T. Florez, and S. J. Allen, Jr., Phys. Rev. Lett. **64**, 471 (1990).
[33]D. Landheer, G. C. Aers, and Z. R. Wasilewski, Superlatt. Microstruct. **11**, 55 (1992).
[34]R. Lake, G. Klimeck, and S. Datta (unpublished).
[35]C. H. Grein, E. Runge, and H. Ehrenreich (unpublished).
[36]M. L. Leadbeater, E. S. Alves, L. Eaves, M. Henini, O. H. Hughes, F. W. Sheard, and G. A. Toombes, Semicond. Sci. Technol. **3**, 1060 (1988).
[37]M. L. Leadbeater, E. S. Alves, F. W. Sheard, L. Eaves, M. Henini, O. H. Hughes, and G. A. Toombes, J. Phys. Condens. Matter. **1**, 10 605 (1989).
[38]M. L. Leadbeater and L. Eaves, Phys. Scri. **T35**, 215 (1991).
[39]M. C. Payne, J. Phys. C **19**, 1145 (1986).
[40]P. J. Turley and S. W. Teitsworth (unpublished).
[41]J. L. Oudar, A. Migus, D. Hulin, G. Grillon, J. Etchepare, and A. Antonetti, Phys. Rev. Lett. **53**, 384 (1987).
[42]S. Das Sarma, in *Hot Carriers in Semiconductor Microstructures,* edited by J. Shah (Academic, Boston, 1991).
[43]R. W. Hamming, *Digital Filters,* 3rd ed. (Prentice-Hall, Englewood Cliffs, NJ, 1989).